Effect of Magnesium Cation on the Interfacial Properties of Aqueous Salt Solutions

Karen M. Callahan,[†] Nadia N. Casillas-Ituarte,[‡] Man Xu,[‡] Martina Roeselová,[§]
Heather C. Allen,[‡] and Douglas J. Tobias*,[†]

AirUCI Environmental Molecular Science Institute and Department of Chemistry, University of California,
Irvine, California 92697, Department of Chemistry, The Ohio State University, 100 West 18th Avenue,
Columbus, Ohio 43210, and Center for Biomolecules and Complex Molecular Systems, Institute of Organic
Chemistry and Biochemistry, Academy of Sciences of the Czech Republic, Flemingovo nam. 2, 16610 Prague 6,
Czech Republic

Sodium chloride solutions have been used extensively as a model of seawater in both theoretical and experimental studies of the chemistry of sea salt aerosol. Many groups have found that chloride anions are present at the air−solution interface. This observation has been important for the development of a mechanism for the heterogeneous production of molecular chlorine from chloride in sea salt aerosol. However, while sodium chloride is a major constituent of seawater, it is by no means the only salt present. Seawater contains one Mg^{2+} for every eight Na^+. Mg^{2+} is naturally occurring in ocean waters from mineral deposits in the Earth's crust and biological sources. Mg^{2+} forms a hexahydrate structure, rather than contact ion pairs with chloride anion, and this impacts the ordering of water in solution. In this study, we use molecular dynamics simulations, ab initio calculations, and vibrational sum frequency generation (SFG) spectroscopy to explore the effect of the Mg^{2+} cation and its tightly bound solvation shell on the surface propensity of chloride, ion−ion interactions, and water structure of the air−solution interface of concentrated chloride salt solutions. In addition, we provide molecular level details that may be relevant to the heterogeneous reactions of chloride in deliquesced sea salt aerosols. In particular, we show that the presence of the divalent Mg^{2+} cation does not modify the surface propensity of chloride compared to Na^+ and hence, its availability to interfacial reaction, although some differences in the behavior of chloride may occur due to specific ion interactions. In this work, we also discuss the SFG free OH band at the surface of salt solutions and conclude that it is often not straightforward to interpret.

1. Introduction

Chlorine radical is responsible for the destruction of ozone in the stratosphere and remote troposphere. In more polluted atmospheres, it reacts predominantly with alkanes and NO, resulting in ozone formation.[1,2] It has been known for half a century that sea salt aerosols in urban atmospheres are deficient in chloride and bromide.[3,4] The depletion of chloride actually occurs via several mechanisms, but most importantly to this study, it was shown that sea salt aerosol is a source of Cl_2 gas, which photolyzes to chlorine radical.[3,5−9] However, the known gas phase and bulk solution reactions of OH radical with aqueous NaCl aerosols could not account for the rate of formation of Cl_2 gas.[10] A heterogeneous reaction, occurring at the particle interface, was proposed, and molecular dynamics (MD) simulations utilizing polarizable potentials for both ions and water showed evidence of chloride at the surface of an aqueous NaCl solution.[11−15] This finding was in contradiction with the theory of Onsager and Samaras,[16] held since the early 20th century, which states that ions are repelled from the liquid−vapor interface by their image charges. However, it was not entirely unprecedented, as the presence of halide ions at the surface of salt solutions had been inferred from reactive uptake experiments,[17] and the presence of bisulfate ion at the

air−water interface had been detected in sum frequency generation measurements.[18] The simulation results have been further substantiated by a variety of experimental methods, including vibrational sum frequency generation,[19−24] second harmonic generation,[25−30] and high pressure X-ray photoelectron spectroscopy.[31,32] Very recently, a new theory was published that demonstrates that ion polarization promotes ion adsorption to the air−water interface.[33]

Seawater is composed of a combination of inorganic salts. After sodium chloride, the next most prominent component of seawater is magnesium chloride,[34] with one $MgCl_2$ for every eight NaCl. Previous theoretical studies of the chloride enhancement at interfaces have not included alkaline earth salts, although aqueous magnesium acetate and magnesium nitrate have been studied.[35] Here we use a combination of MD simulations and vibrational spectroscopic techniques to investigate the effect of magnesium dication in a model seawater aerosol on the availability of chloride for heterogeneous reaction, as well as other factors that may affect the reactivity of chloride. In this paper, we consider chloride concentrations corresponding to near saturation in NaCl (4−5 M). This is actually more concentrated than seawater in the ocean (∼0.5 M) and corresponds to seawater aerosols that have had a chance to undergo evaporation while spending time in the atmosphere.

While not a direct measure of ions at the air−water interface, vibrational sum frequency generation (SFG) has previously been used to probe the structure of water at interfaces. However, the water-stretching region is broad and difficult to interpret because

* To whom correspondence should be addressed. E-mail: dtobias@uci.edu.
† University of California.
‡ The Ohio State University.
§ Academy of Sciences of the Czech Republic.

it is heavily influenced by hydrogen bonding, bending overtones, and concerted motions. The sharp free OH peak (due to nonproton donor OH bonds) near 3700 cm^{-1} has been considered the most easily interpreted part of the water spectrum.[36] It is thought to arise from only the topmost layer of water molecules.[22,36] Hence, one might incorrectly assume that any interfacial concentration gradients and related structure resulting from the introduction of solutes are unimportant to free OH interpretation. In salt solutions, the frequency of the free OH peak appears to be unaffected by the identity of the cation. A decrease in intensity of the 3700 cm^{-1} peak upon the addition of acid or salt is commonly attributed to displacement or rearrangement of water by ions and ion pairs near the surface of water. On the other hand, addition of many salts has also shown little effect on free OH intensity in most cases.[19,37,38] In our MD and SFG investigation of solutions containing magnesium chloride, it became clear that the free OH peak frequency and lack of significant intensity change should be readdressed.

Ab initio calculations at the MP2/aug-cc-pVTZ level suggest that the frequency of free OH differs slightly for interactions of water with chloride, sodium, and other water molecules.[39-41] The asymmetric character of the SFG free OH band supports the presence of multiple components; however, these cannot be fit uniquely and are not completely accounted for by varying the nonresonant SFG contribution. Additionally, ab initio calculations predict that the free OH vibrations of water in the first solvation shell of magnesium experience a more substantial frequency shift to lower energy and do not contribute the 3700 cm^{-1} peak. A peak assigned to the free OH vibration of water molecules in the first solvation shell of Mg^{2+} has recently been observed at 3650 cm^{-1} in SFG spectra of MgCl$_2$ solutions, and its intensity increases with concentration.[42] Although phase-sensitive SFG experiments[23,38] may help to substantiate the identity of this peak, this technique still provides an orientation average and thereby does not completely resolve the interpretation issues.

In light of the complications in the interpretation of SFG spectra, including the free OH region, MD simulations were used in the present work to provide insight into the structure of interfacial water in aqueous salt solutions, as well as the ion positioning and solvation environment in the interfacial region, that is not readily available from experimental probes. MD simulations of MgCl$_2$ solutions in the bulk have been performed previously at a variety of concentrations.[43-49] In addition to classical MD studies, there have been several first principles MD and Monte Carlo simulations of the hydration of Mg^{2+} in small clusters.[50-55] We have tested several standard Mg^{2+} force fields, and we developed a new parametrization for the Mg^{2+} ion suitable for simulations at high salt concentrations in the presence of polarizable water. The development of the Mg^{2+} force field, as well as the motivation for using initial configurations in which the Mg^{2+} ions are fully solvated by water, are discussed in another paper.[56] In short, bulk density and experimental radial distribution functions from X-ray diffraction of aqueous MgCl$_2$[57,58] were used to validate the magnesium force field, and Raman spectra of the Mg$-$OH$_2$ stretch over a range of concentrations were used to show that magnesium has a stable first hydration shell and does not form contact ion pairs.[56] Here, we use the newly developed Mg^{2+} force field to compare the surface properties of aqueous sodium chloride, magnesium chloride, and model seawater solutions with a special interest in potential chloride availability to interfacial reaction.

2. Methods

2.1. Experimental Methods. Vibrational SFG spectroscopy is interface-selective. In the dipole approximation SFG gives a signal when centrosymmetry is broken, such as at an interface. Additionally, in order for a vibration to be SFG active it must be both Raman and infrared (IR) active; i.e., dipole moment and molecular polarizability must change with the vibration. Theoretical details of the sum frequency process are available in the literature.[19,59-62]

SFG spectra of the air$-$liquid interface were acquired using a scanning (SSFG) and a broad bandwidth (BBSFG) spectrometer. Details of these two SFG systems are described elsewhere.[21,63-65] SSFG incident angles of the infrared and visible from the surface normal were 59° and 47°, respectively. BBSFG incident angles of the infrared and visible from the surface normal were 68° and 53°, respectively.

SFG spectra were obtained under the ssp (s for the SFG, s for the 532 nm, and p for the infrared beam) and ppp polarization combinations. The coupling into and out of the surface is optimized for the ppp polarization combination on the BBSFG system with changing the incident angles, and, therefore, these angles were significantly different relative to the SSFG system as stated above. For the SSFG spectra, each data point was acquired using 30 s for the acquisition time. SSFG spectra were normalized by the infrared energy, which was measured in real time with the SFG intensity. BBSFG spectra were normalized to the nonresonant signal from a GaAs crystal. An average of at least two replicate spectra is shown in all cases, and error bars show ±1 standard deviation. In the case of the BBSFG spectra, the data markers are plotted every five data points to improve clarity. Spectra were acquired at ∼22 °C and in a range from 40 to 50% relative humidity. Spectra of the full OH stretch region were obtained[42] to verify that the observed change in dangling OH frequency was not a result of a frequency or bandwidth change in the adjacent interfering vibrational modes.

Magnesium chloride hexahydrate (MgCl$_2$·6H$_2$O; ACS certified) and sodium chloride (NaCl; ACS certified) were obtained from Fisher Scientific. Deionized water was obtained from a Barnstead Nanopure filtration system with a minimum resistivity of 18.2 MΩ·cm. For the sodium chloride solutions, the NaCl salt was placed in a muffle oven (Fisher Scientific, Isotemp Muffle Furnace) at 700 °C for 4 h to eliminate any organic contaminants prior to mixing with Nanopure water to obtain the final concentration. For magnesium chloride, a saturated aqueous solution of MgCl$_2$ was prepared and then filtered through a Whatman Carbon-Cap activated carbon filter to remove organic contaminants. The concentration of the filtered MgCl$_2$ solution was determined by the Mohr method.[66] The concentrated MgCl$_2$ solution was then diluted to the final concentration using Nanopure water. The final concentrations of the salt solutions employed in the SFG experiments were 0.037x (2.1 M) for MgCl$_2$, 0.074x Na, and 0.006x Mg (4.5 M of NaCl plus 0.3 M of MgCl$_2$) for the model seawater solution, and 0.08x (4.9 M) for NaCl, where "x" refers to mole fraction and "M" denotes molarity.

2.2. Computational Methods. The liquid$-$vapor interface of chloride salt solutions was simulated employing a slab geometry in which a unit cell of 30 Å × 30 Å × 100 Å was replicated using three-dimensional periodic boundary conditions. Note that the Z dimension of the cell is elongated orthogonal to the liquid$-$vapor interface, so that a vacuum separates the periodic images in the vertical (Z) direction. During this study we determined that for Z dimensions of the cell greater than 100 Å all differences in properties calculated fall within the

Effect of Mg^{2+} on Aqueous Salt Solutions

J. Phys. Chem. A, Vol. 114, No. 32, 2010 **8361**

TABLE 1: Simulation Force Field Parameters

atom	parameter set	q (e)[a]	α (Å^3)[b]	r_{atom} (Å)[c]	ε (kcal/mol)[d]
Mg^{2+}	Callahan[e]	+2	0.000	1.0600	0.875
Na$^+$	PB[f]	+1	0.240	1.3190	0.130
Cl$^-$	PB[f]	−1	3.250	2.4192	0.100
O	POL3[g]	−0.730	0.528	1.798	0.156
H1, H2	POL3[g]	0.365	0.170	0.0	0.0

[a] Charge or partial charge of atom or ion. [b] Atomic polarizability. [c] Position of the minimum in the Lennard-Jones potential. [d] Lennard-Jones well depth. [e] Callahan et al.[56] [f] Perera and Berkowitz.[68] [g] Caldwell and Kollman.[67]

range of statistical uncertainty. All slab simulations contained 864 water molecules and 96 chloride ions.[67] In addition, the saturated model seawater solution contained 10 magnesium dications (0.011x) and 76 sodium cations (0.080x), the saturated NaCl solution contained 96 sodium cations (0.100x), and the magnesium chloride solution contained 48 magnesium dications (0.053x), These concentrations, which were calculated using the compositions of the entire solution slabs, differ from the concentrations listed above for the SFG experiments. Due to the limited thickness of the aqueous solution slabs in the MD simulations, the surface-to-bulk ratio in the simulated solutions is substantially larger than in the macroscopic experimental systems. The nonuniform distribution of ions occurring in the interfacial region (see below)

thus results in the salt concentration in the interior (bulk) region of the slab being different from the nominal concentration of the solution calculated from the number of ions and water molecules in the simulation box. Therefore, the concentrations of the salt solutions in the SFG experiments were chosen to correspond to the salt concentrations established upon adequate equilibration in the central portion of the simulation slabs.

All of the simulations incorporated the rigid, polarizable POL3 water model[67] and the chloride model of Perera and Berkowitz (PB).[68] Additionally, the sodium model is attributed to Perera and Berkowitz by Peterson et al.[27,68] The magnesium force field used in this paper was reported recently by Callahan et al.[56] The force field parameters are provided in Table 1.

The simulations consisted of 3 ns of equilibration in the NVT ensemble, followed by at least 2 ns of data collection for analysis. The molecular dynamics program employed was Sander in the AMBER 8 suite of programs[69] with a modified calculation of the induced dipoles to avoid polarization catastrophe.[27] The temperature was constrained with a Berendsen thermostat using a 1 ps time constant to obtain an average temperature of 300 K.[70] Particle mesh Ewald summation was used to treat the long-range electrostatic interactions. The real-space part of the Ewald sum and the Lennard-Jones interactions were truncated at 12 Å.[71,72] The time step was 1 fs, and trajectory data were recorded every picosecond. Water bond lengths and angles were constrained using the SHAKE algorithm.[73] VMD[74] was used for the analysis of the trajectories and to prepare the molecular graphics images.

In addition to MD simulations of aqueous solution slabs, ab initio geometry optimizations and frequency calculations were performed on small clusters of water and ions to observe local solvation effects on the OH-stretching frequencies of water. The input structures were obtained from the MD simulations. We employed Gaussian 03 with the MP2 method and the aug-cc-pVTZ basis set to optimize the geometries and compute harmonic vibrational frequencies and IR intensities. Calculations with smaller basis sets were also carried out and found to be identical with previously published results.[75]

3. Results and Discussion

3.1. Vibrational Sum Frequency Generation Spectroscopy and Ab Initio Studies of the Free OH Peak of Water. SFG spectra using ssp and ppp polarization combinations of the magnesium chloride, sodium chloride, and model seawater solutions were acquired in the free OH region with our SSFG and BBSFG spectrometers and are shown in Figure 1a−c. The ssp polarized SSFG and BBSFG spectra reveal a small reduction in the SFG intensity for all salt solutions compared to that of water. With the scanning SFG spectrometer, we resolve a clearer spectral decrease in the corresponding spectra of Figure 1a−c. It is important to note that in lower concentration (∼0.02x) aqueous NaCl solutions, a decrease in free OH peak intensity was not observed previously.[21] The ppp polarized BBSFG spectra of MgCl$_2$ and the model seawater solutions show no
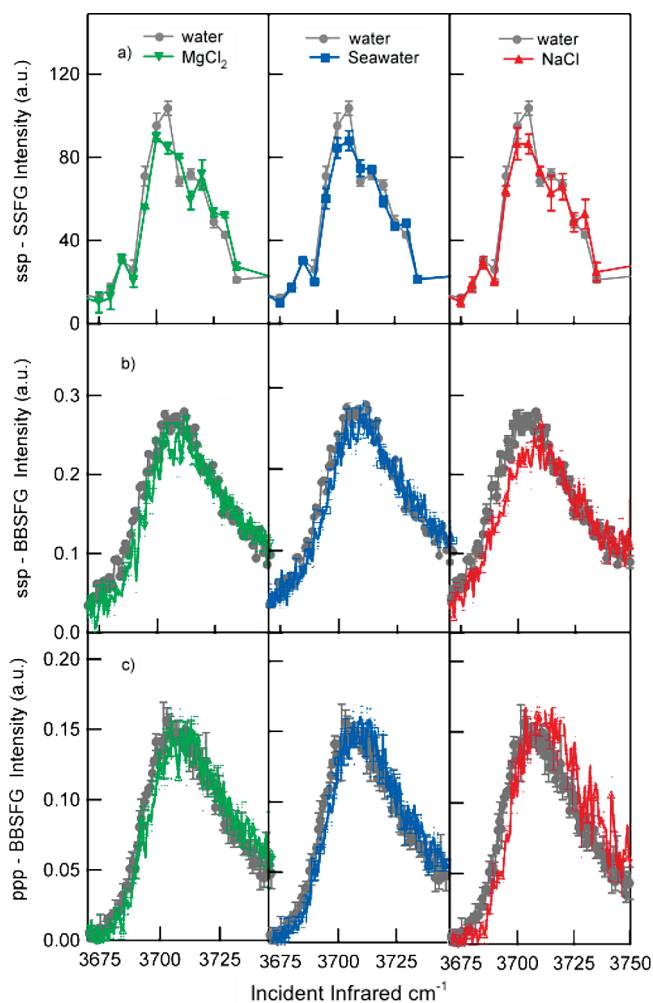
Figure 1. Sum frequency spectra of aqueous MgCl$_2$ (0.037x), model seawater (Na 0.074x and Mg 0.006x), and NaCl (0.08x) in the free OH region using (a, b) ssp polarization combination for the SSFG and the BBSFG systems, respectively, and (c) ppp polarization combination using the BBSFG system. The SFG spectrum of neat water is shown for comparison.

TABLE 2: Harmonic Frequencies and Infrared Intensities of OH Stretches in Water and Water−Ion Clusters[a]

cluster	IR frequency (cm^{-1})	IR intensity (km·mol^{-1})	assignment
(H$_2$O)$_2$	3934	97	acceptor asym. stretch
	3914	115	donor free OH
	3813	11	acceptor sym. stretch
	3717	298	donor bonded OH
Na$^+$·H$_2$O	3892	175	asym. stretch
	3800	54	sym. stretch
Mg^{2+}·H$_2$O	3690	410	asym. stretch
	3635	274	sym. stretch
Mg^{2+}·(H$_2$O)$_2$	3727	369	asym. stretch
	3727	365	asym. stretch
	3669	0.2	sym. stretch
	3664	502	sym. stretch
Cl$^-$·H$_2$O	3892	32	free OH
	3335	1138	bonded OH

[a] Computed at the MP2/aug-cc-pVTZ level of theory.

significant change in intensity relative to that of neat water. However, the BBSFG ppp spectrum of the NaCl solution reveals a very slight intensity enhancement compared to that of neat water (Figure 1c). Using the ssp and ppp intensity ratios, we determined from accepted methods of orientation analysis[76,77] that there was not a significant change in free OH orientation for the salt solutions; however, orientational dynamics can also influence the intensity of the free OH peak.[78,79] Moreover, as inferred from the findings of this paper, if the free OH intensity is not solely from the free OH of the topmost layer of water molecules, and if the free OH peak contains contributions from subsurface solvation shells of the cations, this orientation determination is not valid.

In both ssp and ppp polarized BBSFG spectra, a small blue shift of the free OH relative to that of water is observed. This blue shift increases from 2 cm^{-1} in the MgCl$_2$ solution to 4 cm^{-1} in the NaCl solution. In the ssp polarized SSFG spectra, this blue shift is not as obvious due to the fact that in the SSFG system the infrared frequency is scanned every 5 cm^{-1}. There are several possible causes of this frequency shift. While the nonresonant spectrum is similar for solutions of NaI and neat water, slight changes could be responsible for small shifts in free OH frequency.[38] In the case of MgCl$_2$ solutions, the nonresonant spectrum has never been studied directly and its possible effects on the free OH frequency are currently unknown. An additional source of the shift could come from the effect of interactions of the free OH group with other water molecules of nearest neighbor solvation shells of ions or directly with the ions near it.

To assess the effects of ions on the frequencies and intensities of the water free OH stretches, we performed ab initio calculations on small clusters containing one ion and one or two H$_2$O molecules. Additionally, we performed calculations with monodeuterated water (HOD) to decouple the OH oscillators of a given water molecule. Previously, several different ab initio studies have explored Cl$^-$·H$_2$O,[39,40] Na$^+$·H$_2$O,[41] Mg^{2+}·H$_2$O,[80] and water clusters.[41] Although the calculations presented here are to some extent redundant with previous work, our objective is to present here an analysis of a complete set of results obtained with the same theoretical model.

Harmonic vibrational frequencies and IR intensities obtained at the MP2/aug-cc-pVTZ level for the water dimer and ion−water clusters are presented in Table 2. The frequency of the free OH bond of a water molecule donating a hydrogen bond to the second water molecule in the dimer is 3914 cm^{-1}.

TABLE 3: Harmonic Frequencies and Infrared Intensities of OH and OD Stretches in HOD and HOD−Ion Clusters[a]

| cluster	IR frequency (cm^{-1})	IR intensity (km·mol^{-1})	assignment
HOD	3884	45	OH stretch
	2819	20	OD stretch
Na$^+$·HOD	3847	121	OH stretch
	2794	59	OD stretch
Mg^{2+}·HOD	3663	349	OH stretch
	2663	182	OD stretch

[a] Computed at the MP2/aug-cc-pVTZ level of theory.

In the Cl$^-$·H$_2$O cluster there is a small red shift of the free OH frequency to 3893 cm^{-1}. A similar modest difference in both harmonic and anharmonic frequencies of the free OH in the water dimer and Cl$^-$·H$_2$O was observed previously by Chaban et al.[39] In Na$^+$·H$_2$O the asymmetric stretch occurs at 3892 cm^{-1}, which is similar to the free OH frequency in Cl$^-$·H$_2$O. Thus, we do not expect water interactions with Na$^+$ and Cl$^-$ to shift the free OH frequencies out of the free OH band in the SFG spectra.

In the clusters with Mg^{2+}, we find that there is a considerable red shift of the symmetric and asymmetric stretches of H$_2$O. Comparing Mg^{2+}·H$_2$O to Na$^+$·H$_2$O, the symmetric OH stretch is red-shifted by 165 cm^{-1} and the asymmetric stretch by 202 cm^{-1}. The greater shift in the OH stretch frequencies of water interacting with Mg^{2+} vs Na$^+$ was also observed by Probst and Hermannson.[80] The red shift induced by Mg^{2+} decreases with increasing cluster size, as is evident in the Mg^{2+}·(H$_2$O)$_2$ frequencies given in Table 2.

In solution, interactions of water molecules in the first solvation shell with second shell water molecules or counterions are expected to decouple the symmetric and asymmetric stretches of a water molecule in the first shell. There are technical challenges studying clusters of magnesium with multiple solvent shells, both with ab initio calculations and in experiment. In small clusters (∼6−15 water molecules), a second shell of water around a magnesium or other alkaline earth cation frequently results in the formation of a metal hydroxide and H$_3$O$^+$ in small clusters.[81] This complication to performing experiments with multivalent cations in small water clusters has only recently been overcome.[82,83]

On the theoretical side, widely disparate results are obtained for Mg^{2+} with an incomplete second solvation shell when different theoretical models and initial configurations are employed. It is observed in ab initio calculations of the structure of Mg^{2+}−water clusters that, when a second shell water accepts a single proton from the first shell, formation of a metal hydroxide and hydronium readily occur.[81] However, some authors have obtained a stable structure in which the second shell water molecule accepts protons from two first shell water molecules and does not dissociate.[84,85] Metal hydroxide formation does not seem to occur readily when Mg^{2+} has a complete second solvation shell, and, therefore, one would not expect it to complicate the analysis of vibrational spectra of solutions.[82,86−88]

Our approach to investigating the effects of Mg^{2+} interactions on decoupled free OH stretches was to replace H$_2$O with HOD in the vibrational analysis of the ab initio calculations. The harmonic frequencies of HOD, Na$^+$·HOD, and Mg^{2+}·HOD obtained at the MP2/auc-cc-pVTZ level of theory are listed in Table 3. These data show that there is only a slight (34 cm^{-1}) red shift of the decoupled free OH in Na$^+$·HOD from the frequency of the OH bond in HOD. On the other hand, there is a relatively strong (208 cm^{-1}) red shift of the corresponding mode in Mg^{2+}·HOD.

Effect of Mg²⁺ on Aqueous Salt Solutions

J. Phys. Chem. A, Vol. 114, No. 32, 2010 **8363**
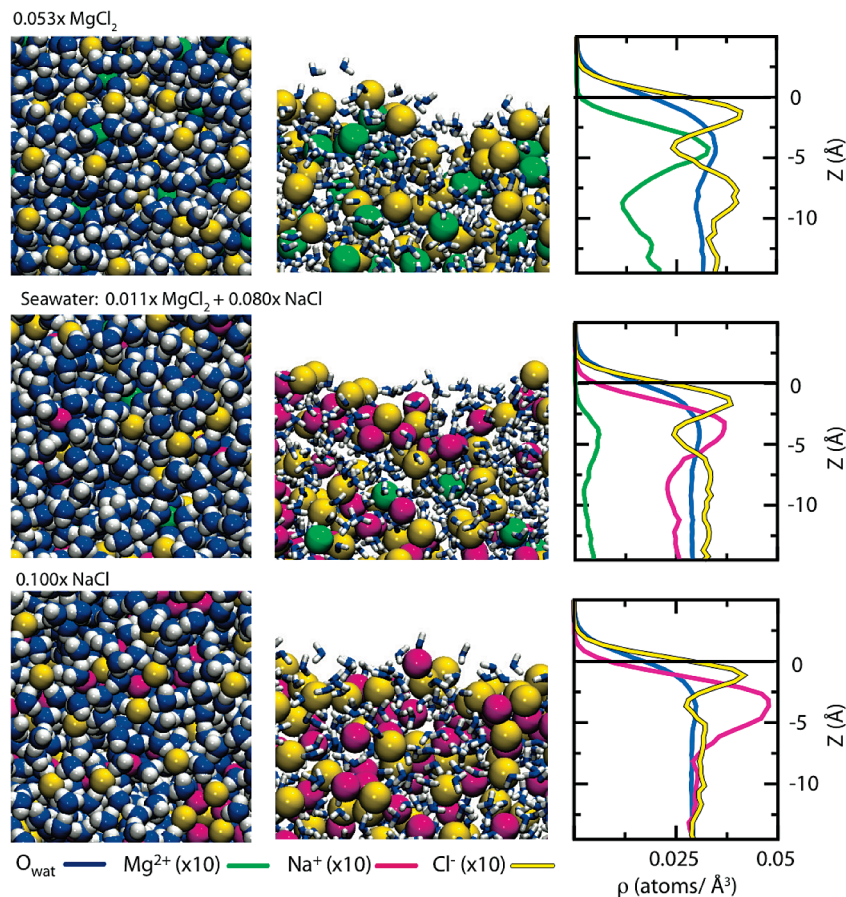
Figure 2. Left, snapshots of the surface of simulation slabs. Center, snapshots of cross-sectional views of the top half of the simulation slabs. Right, number density profiles. Densities are in units of atoms/Å³, and the ion densities are scaled by a factor of 10. The Gibbs dividing surface is set to Z = 0 Å. The colors in the density profiles correspond to the atom colors in the snapshots.

The calculations presented here suggest that the frequencies of the free OH bonds in the first solvation shell of Mg²⁺ could be red-shifted relative to the peak in the free OH band at ∼3700 cm⁻¹. Thus, we conclude that it is possible that Mg²⁺−water interactions could be responsible for a small reduction of intensity in the main free OH peak at ∼3700 cm⁻¹, as was observed in the SFG spectra of the Mg²⁺-containing solutions (Figure 1). This conclusion is supported by the appearance of a new peak at 3650 cm⁻¹ in MgCl₂ solutions, the intensity of which increases with concentration, as has been recently reported elsewhere.[42]

Turning now to the intensities, we find that while the presence of a cation (and particularly Mg²⁺) enhances the intensity of free OH stretches (Tables 2 and 3), the presence of chloride decreases it (Table 2). The reduction in intensity of a free OH in Cl⁻·H₂O compared to a free OH in (H₂O)₂ was also found by Chaban et al.[39] We do not expect, however, the increase of intensity for Mg²⁺·H₂O to show up in the 3700 cm⁻¹ band of the SFG spectrum of Mg²⁺-containing solutions. Rather, we expect Mg²⁺ to reduce the intensity of the free OH band because of the frequency shift noted above.

While the individual contributions of the 3700 cm⁻¹ peak cannot be separated, we do note that both the peak in the salt solutions and that in neat water are asymmetric, and this cannot be fully not accounted for by the nonresonant background. As shown above we expect the contributions from water in the presence of different ions to be inequivalent. Regrettably, this complication makes separation of the number density dependence and orientational dependence of the SFG signal from free OH in our systems complicated and uncertain. Therefore, we

cannot assign the reduction in the ssp spectra of Figure 1a and b to a decrease in the number density of free OH at the surface of the chloride solutions relative to that from the neat water surface. The decreased intensity could be due to interactions of some free OH oscillators with ions rather than simply changes in the actual number of free OH.

3.2. The Composition of the Air−Solution Interfaces. Given the complications of interpreting the experimental SFG spectra in the free OH region presented above, we now turn to molecular dynamics simulations to gain insight into molecular structure at the air−solution interface. Results from interfacial simulations of aqueous magnesium chloride, the mixture of aqueous magnesium and sodium chloride, and aqueous sodium chloride are shown in Figure 2. Snapshots of the top view as well as a cross-sectional view of half of each system are shown on the left side, and number density profiles are shown on the right. The densities of the ions have been scaled by a factor of 10. The Gibbs dividing surface (GDS), which is approximated by the point along the Z axis halfway between where the water density is 10% and 90% of the bulk water density, is set to Z = 0. This is meant to provide a common point of reference for each system and guide the eye for all relevant figures. Ideally, in the central portion of the slab (Z ∼ −15 Å) the density profiles are expected to flatten out, corresponding to a well-established bulk phase in which the molecules no longer feel the interface and molecular distributions and orientations become independent of Z. The slabs of MgCl₂ presented in Figure 2 are not thick enough to support a converged bulk region. It is likely that this is in part due to the large size of the hexa-aquo magnesium complex. The lack of a true aqueous bulk phase does not hinder

8364 *J. Phys. Chem. A, Vol. 114, No. 32, 2010*

Callahan et al.

TABLE 4: Surface Tensions

system	calculated surface tension, γ (dyn/cm)[b]	calculated $\Delta\gamma$ (dyn/cm)[b]	experimental[101] $\Delta\gamma$ (dyn/cm)
neat water[a]	54.7 ± 0.9	−	−
MgCl$_2$ (0.053x)	54.9 ± 1.2	0.2 ± 1.5	6.35 ± 0.30^c
seawater (0.011x MgCl$_2$, 0.080x NaCl)	57.5 ± 2.6	2.8 ± 2.8	−
NaCl (0.100x)	60.2 ± 1.2	5.5 ± 1.5	7.36 ± 0.25^d

[a] The experimental surface tension of neat water is 72.75 dyn/cm at 20 °C.[101] *[b]* All simulation results obtained at 300 K. *[c]* 2.0 *m*, 293 K. *[d]* 4.5 *m*, 293 K.

us in determining, qualitatively, whether chloride adsorbs to the interface in the systems under study, nor in determining similarities and differences in the local structure of water and ions around chloride both near and away from the solution surface. In the remainder of this paper "bulk" is used to mean near the center of the slab.

The density profiles exhibit peaks in the chloride densities just below the GDS, indicating enhancement of the chloride population in the interfacial region. The aqueous MgCl$_2$ solution, the model seawater, and aqueous NaCl solution all show similar chloride surface enhancement. We also note that MgCl$_2$ solution shows a considerable magnesium enhancement near the interface that is nearly twice the bulk concentration. A similar effect is observed in the seawater system. Additionally, there is a second layer of enhanced chloride concentration deeper in the slab for the MgCl$_2$ solution, but not in the solutions containing sodium cations. Thus, in seawater the chloride distribution is affected more strongly by the overwhelming number of sodium cations, rather than the relatively few magnesium cations present.[56]

Surface tension is an experimentally measurable thermodynamic property that provides information on the interfacial composition of aqueous solutions. It is also readily computed from MD simulation data, and comparison of computed values to experimental data is useful for validating the predictions of the simulations. Because most simulation force fields are not capable of accurately reproducing the surface tension of neat water,[12,15,89,90] the surface tension increment, or the change in surface tension with the addition of solute, $\Delta\gamma$, is ordinarily used to validate simulation data. We calculated the surface tension using the following equation

$$\gamma = \frac{1}{2}L_Z \left\langle P_{ZZ} - \frac{1}{2}(P_{XX} + P_{YY}) \right\rangle$$

where L_Z is the height of the box and $P_{\alpha\alpha}$ are the diagonal components of the pressure tensor, and the angular brackets denote a time average. We report the surface tension of water and the salt solutions computed from the MD simulations, along with the corresponding experimental data, in Table 4. The error bars in the simulation data were obtained by the method of blocking transforms.[91]

Although a quantitative comparison is not possible due to differences in concentration and temperature of the simulations and the experiments, at first glance the simulations data are in qualitative agreement with the experimental results: addition of salt results in an increase in surface tension. The surface tension increment predicted by the simulation for NaCl is in good agreement with the experimental data, while that for MgCl$_2$ is substantially too low. The lack of agreement for MgCl$_2$ could reflect inadequacies in the Mg^{2+} force field, or it could be a consequence of a system size artifact. Recent work has shown that the simulated system should be sufficiently large in the direction normal to the interface (Z) to support a well-defined bulk region in order for the computed surface tensions (and
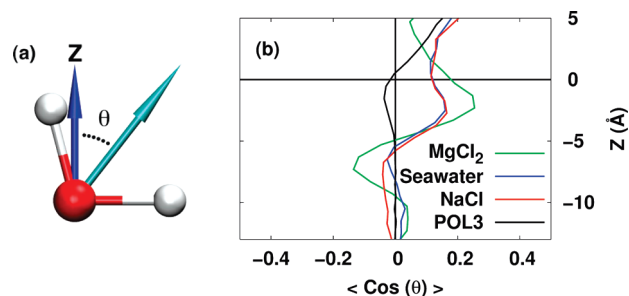

Figure 3. (a) Definition of the angle between the water dipole moment (cyan) and the interface normal (Z axis). (b) Average orientational order parameter of all the water dipoles as a function of depth in the slab. The Gibbs dividing surface is set to $Z = 0$ Å.

surface excesses) to be reliable.[92] As mentioned above, the density profiles in Figure 2 reveal that the bulk region in the systems containing Mg^{2+} is considerably less well-established than in the NaCl solution.

3.3. Structuring and Orientational Order of Interfacial Water Molecules. An orientational order parameter, defined as the average cosine of the angle between a water dipole and the surface normal vector of the slab, is used to enumerate the degree of net orientation of water molecules as a function of depth in the slab. A positive value of $\langle \cos \theta \rangle$ indicates net ordering of water molecules with their dipoles pointing toward the gas phase. Figure 3b shows that the addition of salt causes an increase of the net orientation of water in the interfacial region between $Z = 0$ and $Z = -5$ Å. In addition, in the MgCl$_2$ solution the depth of the oriented region is clearly greater than for neat water, and below $Z = -5$ Å the direction of the net orientation switches. This switch in water orientation corresponds to the enhancement of magnesium concentration at ~ -5 Å (see Figure 2). We conclude that the more ordered first solvation shell of the magnesium has a greater influence on the water orientation than the less ordered first solvation shell of sodium.[50,93,94] As all the solutions exhibit net orientation above -5 Å, we conclude that chloride plays a role in orienting water molecules in this region. In addition, magnesium appears to also influence this region, and the extent of the orientation of the water in the region near -5 Å is greater in the MgCl$_2$ solution compared to the NaCl solution and the model seawater.

In section 3.1, we used ab initio calculations to discuss the effect of ions on water vibration frequencies and intensities. Two additional measures of surface structure that are relevant to the free OH SFG spectrum are the number of free OH oscillators and their net orientation. A free OH bond is, by definition, not a hydrogen bond donor. Here we define hydrogen bonds by distance and angle criteria. We define the distance cutoff as the position of the first minimum in the water H−water O or water H−chloride radial distribution functions. For water−water hydrogen bonds, this gives a cutoff of 2.3−2.4 Å, depending on the particular solution, and 3.0−3.1 Å for water−chloride hydrogen bonds. The angular criteria are chosen so that 95% of the interactions satisfying the distance criteria are accepted as hydrogen bonds. This results in an angular
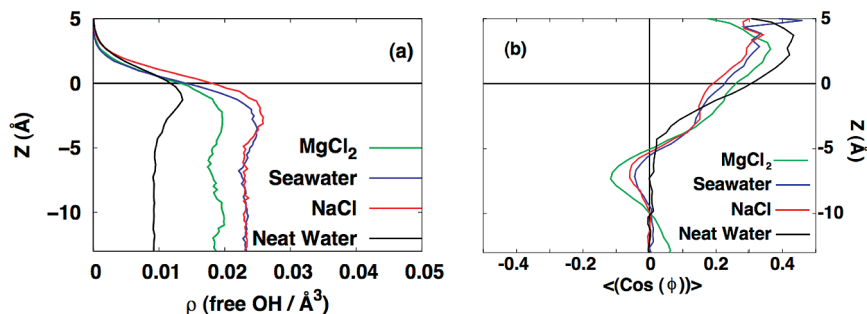
Figure 4. (a) Density of free OH as a function of depth in the slab for simulations of water, NaCl, MgCl$_2$, and model seawater. The Gibbs dividing surface of each system is set to $Z = 0$ Å. The area under each distribution reflects relative concentration differences between the systems. (b) Plot of the average orientational order parameter of water free OH bonds. ϕ is the angle between the O–H vector and the Z axis. Positive values of $\langle\cos(\phi)\rangle$ correspond to the hydrogen atoms pointing to the vapor phase, away from the bulk. Values of $\langle\cos(\phi)\rangle$ near 0 correspond to centrosymmetric conditions.

cutoff corresponding to a 40°–45° deviation from a linear O$_{wat1}$–H$_{wat1}$...O$_{wat2}$ or O$_{wat}$–H$_{wat}$...Cl$^-$ arrangement (again determined independently for each solution). These are similar to criteria used previously, except that it is common to use an angular cutoff of 30° for all systems.[78,95] This definition of free OH is entirely structural. Simulation data was recorded every picosecond; this is greater than the lifetime predicted for the free OH in bulk water (<200 fs) by Eaves et al.; therefore, we cannot calculate the lifetime of the free OH in our simulations.[96]

Figures 4a and 4b show plots of the density and orientational order parameters of the free OH as functions of Z for water and saltwater systems. We see that the presence of salt results in increased concentrations (number densities) of free OH bonds, compared to neat water. While high concentrations of ions at the interface displace some water, and could thus be anticipated to reduce the number density of free OH bonds, the observation of more free OH in the salt solutions versus neat water is expected because ions disrupt the water hydrogen bonding network by orienting water in solvation shells. This is particularly true about the magnesium cation which strongly affects the water structure.[56] The concentration of free OH increases more for sodium chloride and the model seawater solutions than for the magnesium chloride solution, however, as there are far fewer Mg^{2+} in the MgCl$_2$ solution than Na$^+$ in the other solutions. In Figure 4b, we plot the orientational order parameter, $\langle\cos(\phi)\rangle$ for the free O–H bond as a function of depth in the slab, where ϕ is the angle of the free OH relative to the surface normal (the Z axis). A positive value of $\langle\cos(\phi)\rangle$ here means that the free O–H bonds are on average oriented with the H atom pointing toward the vapor phase, whereas a negative value means that the H atoms point into the center of the slab. We would like to point out that this plot gives the average $\cos(\phi)$ value obtained from all free OH bonds at a particular value of Z, including those bonds which will not contribute to the 3700 cm^{-1} peak because of centrosymmetry. Therefore, the absolute values of $\langle\cos(\phi)\rangle$ obtained will be smaller than those inferred from SFG experiments where only free OH bonds in noncentrosymmetric environments contribute to the signal. The curves in Figure 4b have been normalized to remove concentration dependence. The net orientational order was divided by the concentration of free OH as a function of Z. Figure 4b shows that the orientation of free OH has similarities in all systems. Above −5 Å, the H atoms in the free OH bonds point to the vapor phase in all the systems. In the salt solutions there is a narrow region where the free OH orientation has a net orientation toward the center of the slab (negative $\langle\cos(\phi)\rangle$), below which the orientation becomes essentially random ($\langle\cos(\phi)\rangle \sim 0$). The exception to this is the simulation of the MgCl$_2$ solution, which does not reach a region of random
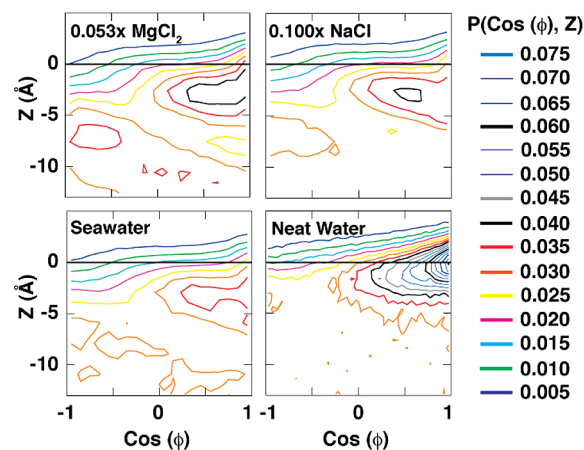

Figure 5. Joint probability distribution of the position in the slab (Z) and of $\cos(\phi)$ of free OH bonds, where ϕ is the angle between the O–H vector and the Z axis. This plot includes number density dependence of free OH bonds. A solid black line indicates the Gibbs dividing surface, set to $Z = 0$ Å for each system. A positive value of $\cos(\phi)$ means that the hydrogen atom of the O–H bond points toward the vapor phase.

orientation. Once again, this indicates that the thickness of the MgCl$_2$ solution slab is too small to support true bulk conditions inside the slab. Nevertheless, for all systems the region with the greatest net water orientation is in the vicinity of and above the GDS, i.e., the topmost layer of water molecules.

Figure 5 shows the probability distribution of the free OH orientations relative to the Z axis as a function of depth. A solid black line at $Z = 0$ denotes the GDS. Figure 5 shows that the largest population of free OH resides around and just below the GDS, with the hydrogen atoms pointing up into the vapor phase. For neat water there is a single region of enhanced free OH near the GDS. For the salt solutions, this peak is less symmetrically shaped, corresponding to a region of enhanced ion concentrations just below the GDS. In neat water, the orientational distribution of free OH more than 10 Å below the GDS becomes smooth. In contrast, for the salt solutions, order persists throughout the slab with alternating layers of H pointing into the vapor phase (positive $\cos(\phi)$) or into the center of the slab (negative $\cos(\phi)$). This subsurface structuring is particularly pronounced in MgCl$_2$ solution; this is likely due to ordering of Mg^{2+} hydrate in the solution.

3.4. Partitioning and Solvation Environment of Chloride at the Air–Solution Interface and Relevance to Heterogeneous Chemistry. In the previous sections we addressed the significant effects of magnesium cation on the structural properties and ordering of water in the interfacial region of salt solutions. Next, we use molecular dynamics to explore the potential effects of magnesium cation in solution on the
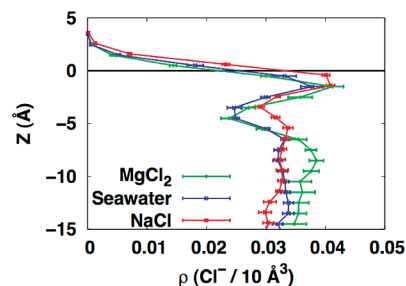
Figure 6. Chloride ion density as a function of depth in the slab for the seawater and saturated NaCl and $MgCl_2$ simulations. The Gibbs dividing surface of each system is set to $Z = 0$ Å. The area under each distribution is equal to 0.5.
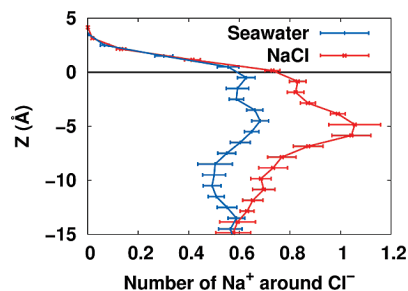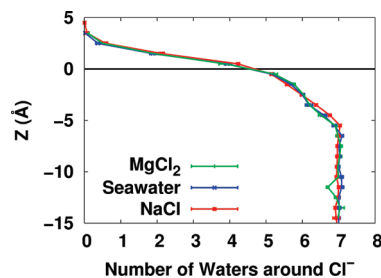

Figure 7. Average coordination numbers of Na^+ around Cl^- as a function of depth in the slab, normalized for the number of Cl^- at each height. The Gibbs dividing surface is set to $Z = 0$ Å.

availability of chloride for heterogeneous reaction at the air–solution surface of seawater aerosols.

Figure 6 gives a direct comparison of the chloride distributions for each system. Error bars are determined using the method of blocking transforms.[91] We find that, while a similar amount of chloride is present at the interface of all the solutions, the depletion of chloride in the subsurface (~-5 Å) is larger for the solutions containing magnesium. The chloride depletion in all the systems corresponds to the region where the cation concentrations are enhanced.

One measure of the availability of chloride anions for reactions with trace gases at the interface is the solvent accessible surface area (SASA).[10] We use the SASA algorithm available in VMD[74,97] with a probe radius of 1.7 Å to represent the approximate size of an OH radical.[10] Standard deviations were determined by the method of blocking transformations.[91] In saturated NaCl solutions approximately $18 \pm 1\%$ of the accessible surface was occupied by Cl^-. The seawater and $MgCl_2$ solutions showed Cl^- SASA of $14 \pm 1\%$ and $20 \pm 2\%$, respectively. In contrast, the fraction of the system surface occupied by the cations is rather small (<4% for Na^+ and <1% for Mg^{2+}).

As shown in a separate study, Mg^{2+} does not form contact ion pairs at the concentration used for the present experiments and simulations.[56] This raises the possibility of differences in Na^+-Cl^- ion pairing behavior of the Cl^- near the interface of seawater and NaCl solutions with similar Cl^- concentrations. Figure 7 shows the average coordination number of Na^+ around Cl^- in the model seawater and NaCl solution. While the pattern of contact ion pairing with respect to distance from the GDS is very similar in both NaCl solution and seawater, there is a greater extent of ion pairing near the surface of the NaCl solution vs seawater system which reflects the greater subsurface population of Na^+ in the former. The increase in contact ion pairing around -5 Å for both NaCl solution and seawater corresponds to the heightened concentration of Na^+ cations and


Figure 8. Average coordination number of water around Cl^- for both seawater and saturated NaCl and $MgCl_2$ solutions as a function of depth in the slab. The Gibbs dividing surface is set to $Z = 0$ Å.

Cl^- anion depletion at that depth. The ion pairing curves near the GDS do not decrease monotonically, following the Na^+ density profile (see Figure 2), but exhibit a secondary maximum at $Z \sim 0$ Å. This corresponds to a true enhancement of Na^+-Cl^- ion pairing at the interface likely because less complete hydration reduces solvent screening of ion charges. We note, in addition, that the increased interfacial ion pairing may stabilize chloride ions at the salt solution surfaces.

Figure 8 shows the average coordination number of water molecules around Cl^- in saturated NaCl and $MgCl_2$ solutions as well as in model seawater as a function of depth in the slab. The solvent shell is defined by the number of O_{water} within the first minimum of the Cl^-–O_{water} radial distribution (4.0 Å). This includes four to six water molecules donating hydrogens to the chloride, and additional water molecules that simultaneously donate and accept protons to/from first shell waters. While the presence of ion pairs to sodium reduces the number of water molecules donating hydrogen to chloride (not shown), it can be seen that there is no substantial effect of Mg^{2+} vs Na^+ ions on the total number of water molecules in the first solvation shell of Cl^- as the individual chloride anions are equally solvated in all three systems, and the hydration of Cl^- follows the same trend as it gets reduced when approaching the interface.

While chloride ions are negatively charged, and therefore repel each other, two chloride ions are required to form molecular chlorine. The exact mechanism by which the reaction occurs at aqueous interfaces is still under study.[98,99] Reaction with OH radical to form chlorine gas may be facilitated if the two chloride ions required are in close proximity. Differences in how Mg^{2+} and Na^+ interact with chloride may cause a difference in the distribution of chloride ions around each other. In Figure 9, we present radial distribution functions (RDF) of Cl^- around Cl^- for the three solutions, separately for the interface and for the bulk. We define the interface to be the region where the central Cl^- of the RDF is within 1 Å of the GDS, while for the bulk we stipulate that the central Cl^- of the RDF must be in the middle 14 Å of the slab. All of the salt solutions show a strong Cl^-–Cl^- correlation from 4 to 6 Å throughout the slab, corresponding to solvent-separated or sodium-separated chloride ions. There is no significant effect of the different cations on the most probable distance between chloride ions, but there is an effect on the relative strength of the correlation throughout the slab. When comparing the maxima of the individual curves at ~4.5 Å, we see that at the interface the correlation is stronger in the model seawater and NaCl solutions than in the $MgCl_2$ solution, whereas the $MgCl_2$ solution shows the highest correlation in the bulk. The greater correlation of chloride ions at the surface in the sodium containing solutions appears to be related to the ability of sodium and chloride to form contact ion pairs, which is increased in the interfacial region (cf. Figure 7 and discussion thereof in the text).

Effect of Mg²⁺ on Aqueous Salt Solutions

J. Phys. Chem. A, Vol. 114, No. 32, 2010 **8367**
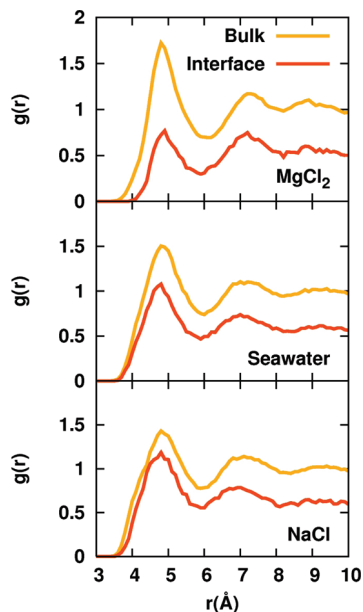
Figure 9. Radial distributions of Cl⁻ around Cl⁻ for the bulk (orange) and at the interface (red). The interface radial distributions do not go to 1 as $r \rightarrow \infty$ because of density inhomogeneity.

4. Conclusions

Studies of the air−solution interfaces of sodium chloride, magnesium chloride, and model seawater solutions were conducted using molecular dynamics and vibrational sum frequency generation spectroscopy. The chosen concentrations, corresponding to near saturation in NaCl, were higher than for water in the ocean in order to model atmospheric aerosols that have undergone evaporation. MD simulations probed several properties of the salt solutions that could be relevant to the reactivity of surface chloride with atmospheric trace gases (e.g., OH radical) but are not readily observable through experiments. All three salt solutions showed similar interfacial enhancement of chloride ion. This suggests that magnesium and sodium have a similar effect on chloride ion enhancement at air−solution interfaces and supports the use of aqueous NaCl as a model of sea salt aerosols, as well as the use of MgCl₂ as a method of adding moisture to NaCl particles.[10,100] However, the inability of magnesium to form contact ion pairs with chloride results not only in decreased ion pairing of chloride in seawater and an essentially complete absence of ion pairing in MgCl₂ solutions, but also in reduced self-correlation among chloride ions near the air−solution interface in the MgCl₂ solution. Additionally, while addition of either salt (NaCl or MgCl₂), or both, results in increased net orientation (decreased centrosymmetry) of both the water dipole and the free OH compared to neat water, this effect is far stronger in the magnesium chloride solution than in the others. This is particularly observed in the strongly held first solvation shell.

While MD simulations predict an increase in the number of free OH upon addition of either salt, a slight decrease in the free OH intensity is observed in the SFG spectra. However, if the free OH peak were solely representative of free OH at the topmost surface of the solutions, a much larger SFG intensity decrease would be expected because of displacement by ions. Ab initio calculations on ion−water clusters showed that ions influence the IR frequencies and intensities of OH stretches. Since SFG is subject to both Raman and IR transition strengths, the changes in the computed IR frequencies and intensities suggest that not all free OH should be expected to contribute equally to the peak in the spectrum at ∼3700 cm⁻¹.

In conclusion, the surface propensity of chloride in NaCl, MgCl₂, and the model seawater solutions was found to be similar, but differences in the behavior of chloride may arise from specific ion interactions in the various solutions.

References and Notes

(1) Finlayson-Pitts, B. J.; Hemminger, J. C. *J. Phys. Chem. A* **2000**, *104*, 11463.
(2) Finlayson-Pitts, B. J. *Chem. Rev.* **2003**, *103*, 4801.
(3) Cicerone, R. J. *Rev. Geophys. Space Phys.* **1981**, *19*, 123.
(4) Jung, C. E. *Tellus* **1956**, *8*, 127.
(5) Robbins, R. C.; Cadle, R. D.; Eckhardt, D. L. *J. Atmos. Chem.* **1959**, *16*, 53.
(6) Finlayson-Pitts, B. J.; Ezell, M. J.; Pitts, J. N. *Nature* **1989**, *337*, 241.
(7) Finlayson-Pitts, B. J. *Nature* **1983**, *306*, 676.
(8) Martens, C. S.; Wesolowski, J. J.; Harriss, R. C.; Kaifer, R. *J. Geophys. Res.* **1973**, *78*, 8778.
(9) Dasgupta, P. K.; Campbell, S. W.; Al-Horr, R. S.; Ullah, S. M. R.; Li, J.; Amalfitano, C.; Poor, N. D. *Atmos. Environ.* **2007**, *41*, 4242.
(10) Knipping, E. M.; Lakin, M. J.; Foster, K. L.; Jungwirth, P.; Tobias, D. J.; Gerber, R. B.; Dabdub, D.; Finlayson-Pitts, B. J. *Science* **2000**, *288*, 301.
(11) Jungwirth, P.; Tobias, D. J. *J. Phys. Chem. B* **2000**, *104*, 7702.
(12) Jungwirth, P.; Tobias, D. J. *J. Phys. Chem. B* **2001**, *105*, 10468.
(13) Jungwirth, P.; Tobias, D. J. *J. Phys. Chem. A* **2002**, *106*, 379.
(14) Jungwirth, P.; Tobias, D. J. *J. Phys. Chem. B* **2002**, *106*, 6361.
(15) Jungwirth, P.; Tobias, D. J. *Chem. Rev.* **2006**, *106*, 1259.
(16) Onsager, L.; Samaras, N. N. T. *J. Chem. Phys.* **1934**, *2*, 528.
(17) Hu, J. H.; Shi, Q.; Davidovits, P.; Worsnop, D. R.; Zahniser, M. S.; Kolb, C. E. *J. Phys. Chem.* **1995**, *99*, 8768.
(18) Baldelli, S.; Schnitzer, C.; Shultz, M. J.; Campbell, D. J. *J. Phys. Chem. B* **1997**, *101*, 10435.
(19) Gopalakrishnan, S.; Liu, D.; Allen, H. C.; Kuo, M.; Shultz, M. J. *Chem. Rev.* **2006**, *106*, 1155.
(20) Mucha, M.; Frigato, T.; Levering, L. M.; Allen, H. C.; Tobias, D. J.; Dang, L. X.; Jungwirth, P. *J. Phys. Chem. B* **2005**, *109*, 7617.
(21) Liu, D.; Ma, G.; Levering, L. M.; Allen, H. C. *J. Phys. Chem. B* **2004**, *108*, 2252.
(22) Schnitzer, C.; Baldelli, S.; Shultz, M. J. *J. Phys. Chem. B* **2000**, *104*, 585.
(23) Tian, C.; Ji, N.; Waychunas, G. A.; Shen, Y. R. *J. Am. Chem. Soc.* **2008**, *130*, 13033.
(24) Feng, R.-r.; Bian, H.-t.; Wang, H.-f. *J. Chem. Phys.* **2009**, *130*, 134710(6).
(25) Petersen, P. B.; Johnson, J. C.; Knutsen, K. P.; Saykally, R. J. *Chem. Phys. Lett.* **2004**, *397*, 46.
(26) Petersen, P. B.; Saykally, R. J. *Chem. Phys. Lett.* **2004**, *397*, 51.
(27) Petersen, P. B.; Saykally, R. J.; Mucha, M.; Jungwirth, P. *J. Phys. Chem. B* **2005**, *109*, 10915.
(28) Petersen, P. B.; Saykally, R. J. *J. Am. Chem. Soc.* **2005**, *127*, 15446.
(29) Petersen, P. B.; Saykally, R. J. *Annu. Rev. Phys. Chem.* **2006**, *57*, 333.
(30) Petersen, P. B.; Saykally, R. J. *J. Phys. Chem. B* **2006**, *110*, 14060.
(31) Ghosal, S.; Hemminger, J. C.; Bluhm, H.; Mun, B. S.; Hebenstreit, E. L. D.; Ketteler, G.; Ogletree, D. F.; Requejo, F. G.; Salmeron, M. *Science* **2005**, *307*, 563.
(32) Brown, M. A.; D'Auria, R.; Kuo, I.-F. W.; Krisch, M. J.; Starr, D. E.; Bluhm, H.; Tobias, D. J.; Hemminger, J. C. *Phys. Chem. Chem. Phys.* **2008**, *10*, 4778.
(33) Levin, Y. *Phys. Rev. Lett.* **2009**, *102*, 147803(4).
(34) *CRC Handbook of Chemistry and Physics*, 77th ed.; CRC Press: Boca Raton, FL, 1996.
(35) Minofar, B.; Vácha, R.; Wahab, A.; Mahiuddin, S.; Kunz, W.; Jungwirth, P. *J. Phys. Chem. B* **2006**, *110*, 15939.

(36) Shultz, M. J.; Schnitzer, C.; Simonelli, D.; Baldelli, S. *Int. Rev. Phys. Chem.* **2000**, *19*, 123.

(37) Richmond, G. L. *Chem. Rev.* **2002**, *102*, 2693.

(38) Ji, N.; Ostroverkhov, V.; Tian, C. S.; Shen, Y. R. *Phys. Rev. Lett.* **2008**, *100*, 096102/1.

(39) Chaban, G.; Jung, J. O.; Gerber, R. B. *J. Phys. Chem. A* **2000**, *104*, 2772.

(40) Roscioli, J. R.; Diken, E. G.; Johnson, M. A.; Horvath, S.; McCoy, A. B. *J. Phys. Chem. A* **2006**, *110*, 4943.

(41) Miller, D. J.; Lisy, J. M. *J. Am. Chem. Soc.* **2008**, *130*, 15393.

(42) Casillas-Ituarte, N. N.; Callahan, K. M.; Tang, C. Y.; Chen, X.; Roeselová, M.; Tobias, D. J.; Allen, H. C. *Proc. Natl. Acad. Sci. U.S.A.* **2010**, *107*, 6616.

(43) Dietz, W.; Riede, W. O.; Heinzinger, K. *Z. Naturforsch.* **1982**, *37a*, 1038.

(44) Bock, C.; Markham, G.; Katz, A.; Glusker, J. *Theor. Chem. Acc.* **2006**, *115*, 100.

(45) Guàrdia, E.; Sesé, G.; Padró, J. A.; Kalko, S. G. *J. Solution Chem.* **1999**, *28*, 1113.

(46) Szász, G. I.; Dietz, W.; Heinzinger, K.; Pálinkás, G.; Radnai, T. *Chem. Phys. Lett.* **1982**, *92*, 388.

(47) Pálinkás, G.; Radnai, T.; Dietz, W.; Szász, G. I.; Heinzinger, K. *Z. Naturforsch.* **1982**, *37a*, 1049.

(48) Heinzinger, K. *Physica* **1985**, *131B*, 196.

(49) Zapalowski, M.; Bartczak, W. M. *Res. Chem. Intermed.* **2001**, *27*, 855.

(50) Lightstone, F. C.; Schwegler, E.; Hood, R. Q.; Gygi, F.; Galli, G. *Chem. Phys. Lett.* **2001**, *343*, 549.

(51) Krekeler, C.; Delle Site, L. *J. Phys.: Condens. Matter* **2007**, *19*, 192101 (7 pp).

(52) Tongraar, A.; Rode, B. M. *Chem. Phys. Lett.* **2005**, *409*, 304.

(53) Tongraar, A.; Rode, B. M. *Chem. Phys. Lett.* **2001**, *346*, 485.

(54) Ikeda, T.; Boero, M.; Terakura, K. *J. Chem. Phys.* **2007**, *127*, 074503.

(55) Tofteberg, T.; Öhrn, A.; Karlström, G. *Chem. Phys. Lett.* **2006**, *429*, 436.

(56) Callahan, K. M.; Casillas-Ituarte, N. N.; Roeselová, M.; Allen, H. C.; Tobias, D. J. *J. Phys. Chem. A* **2010**, *114*, 5141.

(57) Caminiti, R.; Licheri, G.; Piccaluga, G.; Pinna, G. *J. Appl. Crystallogr.* **1979**, *12*, 34.

(58) Caminiti, R.; Licheri, G.; Piccaluga, G.; Pinna, G. *Chem. Phys. Lett.* **1977**, *47*, 275.

(59) Shen, Y. R. *The Principles of Nonlinear Optics*; John Wiley and Sons: New York, 1984.

(60) Lambert, A. G.; Davies, P. B. *Appl. Spectrosc. Rev.* **2005**, *40*, 103.

(61) Moad, A. J.; Simpson, G. J. *J. Phys. Chem. B* **2004**, *108*, 3548.

(62) Hirose, C.; Akamatsu, N.; Domen, K. *Appl. Spectrosc.* **1992**, *42*, 1051.

(63) Harper, K.; Minofar, B.; Sierra-Hernandez, M. R.; Casillas-Ituarte, N. N.; Roeselová, M.; Allen, H. C. *J. Phys. Chem. A* **2009**, *113*, 2015.

(64) Gang, M.; Allen, H. C. *Langmuir* **2006**, *22*, 5341.

(65) Tang, C. Y.; Allen, H. C. *J. Phys. Chem. A* **2009**, *113*, 7383.

(66) Kraemer, E. O.; Stamm, A. J. *J. Am. Chem. Soc.* **1924**, *46*, 2707.

(67) Caldwell, J. W.; Kollman, P. A. *J. Phys. Chem.* **1995**, *99*, 6208.

(68) Perera, L.; Berkowitz, M. L. *J. Chem. Phys.* **1991**, *95*, 1954.

(69) Case, D. A.; Darden, T. A.; Cheatham, T. E., III; Simmerling, C. L.; Wang, J.; Duke, R. E.; Luo, R.; Merz, K. M.; Wang, B.; Pearlman, D. A.; Crowley, M.; Brozell, S.; Tsui, V.; Gohlke, H.; Mongan, J.; Hornak, V.; Cui, G.; Beroza, P.; Schafmeister, C.; Caldwell, J. W.; Ross, W. S.; Kollman, P. A. University of California, San Francisco, CA, 2004.

(70) Berendsen, H. J. C.; Postma, J. P. M.; van Gunsteren, W. F.; DiNola, A.; Haak, J. R. *J. Chem. Phys.* **1984**, *81*, 3684.

(71) Darden, T.; York, D.; Pedersen, L. *J. Chem. Phys.* **1993**, *98*, 10089.

(72) Essmann, U.; Perera, L.; Berkowitz, M. L.; Darden, T.; Lee, H.; Pedersen, L. G. *J. Chem. Phys.* **1995**, *103*, 8577.

(73) Ryckaert, J. P.; Ciccotti, G.; Berendsen, H. J. C. *J. Comput. Phys.* **1977**, *23*, 327.

(74) Humphrey, W.; Dalke, A.; Schulten, K. *J. Mol. Graphics* **1996**, *14*, 33.

(75) Pye, C. C.; Rudolph, W. W. *J. Phys. Chem. A* **1998**, *102*, 9933.

(76) Wei, X.; Shen, Y. R. *Phys. Rev. Lett.* **2001**, *86*, 4799.

(77) Gan, W.; Wu, D.; Zhang, Z.; Feng, R. R.; Wang, H. F. *J. Chem. Phys.* **2006**, *124*, 114705(15).

(78) Walker, D. S.; Hore, D. K.; Richmond, G. L. *J. Phys. Chem. B* **2006**, *110*, 20451.

(79) Fourkas, J. T.; Walker, R. A.; Can, S. Z.; Gershgoren, E. *J. Phys. Chem. C* **2007**, *111*, 8902.

(80) Probst, M. M.; Hermansson, K. *J. Chem. Phys.* **1992**, *96*, 8995.

(81) Beyer, M.; Williams, E. R.; Bondybey, V. E. *J. Am. Chem. Soc.* **1999**, *121*, 1565.

(82) Bush, M. F.; O'Brien, J. T.; Prell, J. S.; Wu, C.-C.; Saykally, R. J.; Williams, E. R. *J. Am. Chem. Soc.* **2009**, *131*, 13270.

(83) Bush, M. F.; Saykally, R. J.; Williams, E. R. *ChemPhysChem* **2007**, *8*, 2245.

(84) Adrian-Scotto, M.; Mallet, G.; Vasilescu, D. *J. Mol. Struct.* **2005**, *728*, 231.

(85) Markham, G.; Glusker, J.; Bock, C. *J. Phys. Chem. B* **2002**, *106*, 5118.

(86) Reinhard, B. M.; Niedner-Schatteburg, G. *Phys. Chem. Chem. Phys.* **2002**, *4*, 1471.

(87) Berg, C.; Achatz, U.; Beyer, M.; Joos, S.; Albert, G.; Schindler, T.; Niedner-Schatteburg, G.; Bondybey, V. E. *Int. J. Mass Spectrom. Ion Proc.* **1997**, *167−168*, 723.

(88) Berg, C.; Beyer, M.; Achatz, U.; Joos, S.; Niedner-Schatteburg, G.; Bondybey, V. E. *Chem. Phys.* **1998**, *239*, 379.

(89) Vega, C.; de Miguel, E. *J. Chem. Phys.* **2007**, *126*, 154707 (10).

(90) Garrett, B. C.; Schenter, G. K.; Morita, A. *Chem. Rev.* **2006**, *106*, 1355.

(91) Flyvbjerg, H.; Petersen, H. G. *J. Chem. Phys.* **1989**, *91*, 461.

(92) D'Auria, R.; Tobias, D. J. *J. Phys. Chem. A* **2009**, *113*, 7286.

(93) Cappa, C. D.; Smith, J. D.; Wilson, K. R.; Messer, B. M.; Gilles, M. K.; Cohen, R. C.; Saykally, R. J. *J. Phys. Chem. B* **2005**, *109*, 7046.

(94) Cappa, C. D.; Smith, J. D.; Messer, B. M.; Cohen, R. C.; Saykally, R. J. *J. Phys. Chem. B* **2006**, *110*, 5301.

(95) Thomas, J. L.; Roeselová, M.; Dang, L. X.; Tobias, D. J. *J. Phys. Chem. A* **2007**, *111*, 3091.

(96) Eaves, J. D.; Loparo, J. J.; Fecko, C. J.; Roberts, S. T.; Tokmakoff, A.; Geissler, P. L. *Proc. Natl. Acad. Sci. U.S.A.* **2005**, *102*, 13019.

(97) Varshney, A.; Brooks, F. P.; Wright, W. V. *IEEE Comput. Graphics Appl.* **1994**, *14*, 19.

(98) D'Auria, R.; Kuo, I. F. W.; Tobias, D. J. *J. Phys. Chem. A* **2008**, *112*, 4644.

(99) Valiev, H.; D'Auria, R.; Tobias, D. J.; Garrett, B. C. *J. Phys. Chem. A* **2009**, *113*, 8823.

(100) Shaka', H.; Robertson, W. H.; Finlayson-Pitts, B. J. *Phys. Chem. Chem. Phys.* **2007**, *9*, 1980.

(101) *International Critical Tables of Numerical Data, Physics, Chemistry, and Technology*, 1st ed.; McGraw-Hill Book Co.: New York, 1926−1930.